



Updated Mass, Eccentricity, and Tidal Heating Constraints for the Earth-sized Planet LP 791-18 d

Michael Greklek-McKeon¹ , Heather A. Knutson¹ , W. Garrett Levine² , Renyu Hu^{1,3} , Morgan Saidel¹ , Jonathan Gomez Barrientos¹ , Konstantin Batygin¹ , and Björn Benneke^{4,5}

¹ Division of Geological and Planetary Sciences, California Institute of Technology, Pasadena, CA 91125, USA; michael@caltech.edu

² Department of Astronomy, Yale University, New Haven, CT 06511, USA

³ Jet Propulsion Laboratory, California Institute of Technology, 4800 Oak Grove Drive, Pasadena, CA 91109, USA

⁴ Department of Physics and Trottier Institute for Research on Exoplanets, Université de Montréal, Montreal, QC, Canada

⁵ Department of Earth, Planetary, and Space Sciences, University of California, Los Angeles, CA 90095, USA

Received 2025 January 30; revised 2025 April 25; accepted 2025 May 5; published 2025 July 3

Abstract

LP 791-18 d is a temperate Earth-sized planet ($R_P = 1.03 R_\oplus$, $P = 2.76$ days) orbiting a late M dwarf, with an interior super-Earth (LP 791-18 b, $R_P = 1.2 R_\oplus$, $P = 0.95$ days) and an exterior sub-Neptune (LP 791-18 c, $R_P = 2.5 R_\oplus$, $P = 4.99$ days). Dynamical interactions between LP 791-18 d and c produce transit timing variations (TTVs) that can be used to constrain the planet masses and eccentricities. These interactions can also force a non-zero eccentricity for LP 791-18 d, which raises its internal temperature through tidal heating and could drive volcanic outgassing. We present three new transit observations of LP 791-18 c with Palomar/WIRC, including the most precise TTV measurements (<6 s uncertainty) of this planet to date. We fit these times with a TTV model to obtain updated constraints on the mass, eccentricity, and tidal heat flux of LP 791-18 d. We reduce the mass uncertainty by more than a factor of two ($M_d = 0.91 \pm 0.19 M_\oplus$). We perform an updated fit assuming tidally damped free eccentricities and find $e_d = 0.0011_{-0.0008}^{+0.0010}$ and $e_c = 0.0001 \pm 0.0001$, consistent with circular orbits. We find that the observed TTVs are not sensitive to $e \leq \sim 0.01$. Without a tidally damped eccentricity prior, $e_d = 0.056_{-0.014}^{+0.015}$, much higher than the eccentricity predicted by n-body simulations incorporating the effects of dynamical excitation and tidal damping. We predict the timing offset relative to the prediction for a circular orbit of upcoming JWST secondary eclipse observations for LP 791-18 d ($\Delta t = -0.2_{-2.7}^{+2.0}$ minutes and $\Delta t = -117_{-47}^{+41}$ minutes for the damped and undamped eccentricity cases, respectively), which could tightly constrain the eccentricity and tidal quality factor of this Earth-sized exoplanet.

Unified Astronomy Thesaurus concepts: [Transit timing variation method \(1710\)](#); [Exoplanet dynamics \(490\)](#); [Eccentricity \(441\)](#); [Exoplanet tides \(497\)](#); [Transits \(1711\)](#)

1. Introduction

Small planets transiting low-mass stars enable the detailed study of exoplanets with Earth-like sizes and compositions. Of these planets, temperate worlds transiting cooler and smaller late M stars offer the rare opportunity to study the atmospheres of these Earth-sized planets with the James Webb Space Telescope (JWST). Planets orbiting smaller stars have relatively stronger atmospheric transmission features, making even compact, high mean-molecular weight atmospheres accessible to characterization with JWST (e.g., A. Banerjee et al. 2024; A. Gressier et al. 2024; C. Piaulet-Ghorayeb et al. 2024). Yet, despite extensive ongoing searches, there are currently only four known temperate (<400 K), Earth-sized (<1.1 R_\oplus) transiting planets outside of the TRAPPIST-1 system (NASA Exoplanet Archive 2024a). This population includes a recently discovered Earth-sized planet transiting the M6 star LP 791-18 (M. S. Peterson et al. 2023, hereafter referred to as P23). LP 791-18 d has a radius of $1.03 \pm 0.04 R_\oplus$, an orbital period of 2.75 days, and an equilibrium temperature of 396 K, with a tidally locked permanent night-side that could plausibly allow for water condensation (P23). It is part of a three planet system, with a sub-Neptune ($2.5 R_\oplus$,

$P = 4.99$ days) LP 791-18 c on an exterior orbit, and a super-Earth ($1.2 R_\oplus$, $P = 0.95$ days) LP 791-18 b on an interior orbit (I. J. M. Crossfield et al. 2019).

It is often challenging to measure masses for small planets using the radial velocity technique (e.g., D. A. Fischer et al. 2016; J. T. Wright 2018; F. Dai et al. 2024). Fortunately, dynamical interactions between planets in the LP 791-18 system cause detectable transit timing variations (TTVs) that can be used to constrain the planet masses and orbital eccentricities. P23 carried out an extensive transit follow-up campaign to characterize the TTVs in this system, including a near-continuous 172 hr Spitzer observation that was conducted in 2019 to confirm the existence of LP 791-18 d. These data were supplemented by an additional 19 ground-based transits of planet c and 40 transits of planet d executed on 0.4–1.9 m facilities including LCOGT, EDEN, ExTrA, SPECULOOS, TRAPPIST, MEarth, MuSCAT, and MuSCAT2. These observations resulted in the detection of TTV signals with amplitudes of ~ 2.5 and ~ 0.5 minute for planets c and d, respectively. P23 also found that there was a strong “chopping” TTV signal in their data, indicating that the planets in this system have relatively large mass ratios and/or eccentric orbits (Y. Lithwick et al. 2012; K. M. Deck et al. 2014). They found that LP 791-18 c has a mass of $7.1 \pm 0.7 M_\oplus$ and LP 791-18 d has a mass of $0.9_{-0.4}^{+0.5} M_\oplus$, and predicted with dynamical simulations that LP 791-18 d maintains a nonzero forced eccentricity of ~ 0.0015 that is



Original content from this work may be used under the terms of the [Creative Commons Attribution 4.0 licence](#). Any further distribution of this work must maintain attribution to the author(s) and the title of the work, journal citation and DOI.

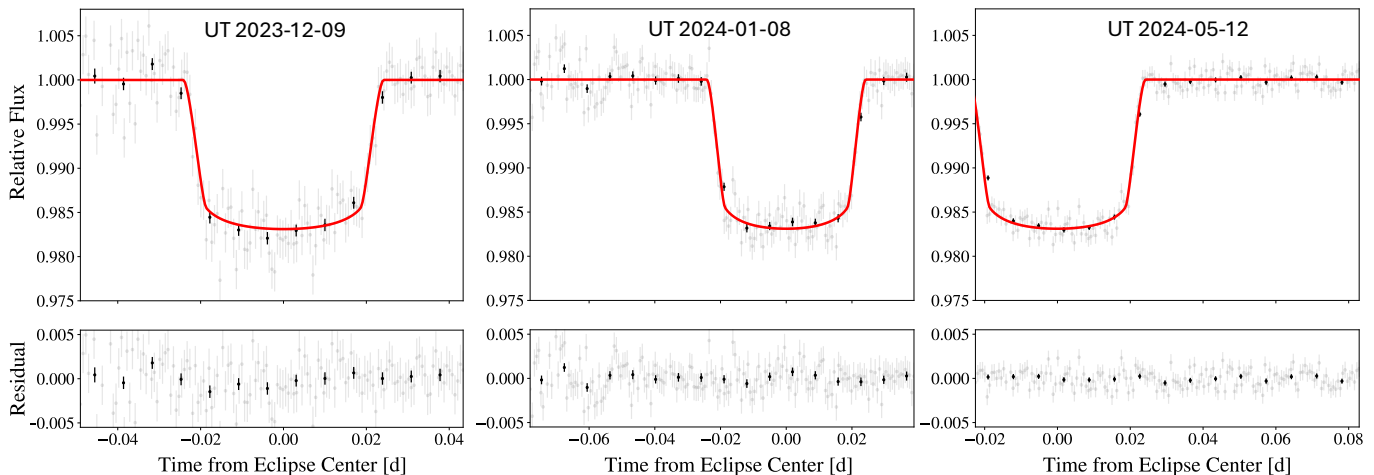


Figure 1. Detrended Palomar/WIRC light curves for the three transit observations of LP 791-18 c (upper panels) and residuals after the best-fit transit light curve has been subtracted (lower panels). Unbinned data are shown as gray circles, with 10 minute binned points overplotted as black circles. The best joint-fit transit models are overplotted as red lines, with red shading to indicate the 1σ uncertainties on the transit shape.

stable long term over the system age due to dynamical interactions with the nearby orbit of the more massive LP 791-18 c.

LP 791-18 d's relatively close-in orbit means that this tiny eccentricity of 0.0015 has an outsized impact on the planet's overall energy budget. Tidal heating in rocky planets impacts interior ice and silicate melting, surface temperature, atmospheric properties, and potential habitability (B. Jackson et al. 2008; L. C. Quick et al. 2020; D. Z. Seligman et al. 2024). If LP 791-18 d has an Earth-like composition and tidal quality factor, the implied tidal heat flux from an eccentricity of 0.0015 is similar to that of Jupiter's moon Io, the most volcanically active body in the solar system (P23). This has significant implications for the atmosphere of LP 791-18 d, which may be dominated by volcanically produced gases. Recent JWST/NIRSpec/NIRISS transmission spectroscopy of the $1.58 R_\oplus$ planet L 98-59 d indicated that this planet may host a sulfur-rich atmosphere, potentially due to volcanic outgassing (A. Banerjee et al. 2024; A. Gressier et al. 2024). Like LP 791-18 d, L 98-59 d also has a nonzero eccentricity ($0.074^{+0.057}_{-0.046}$) that has been suggested as a potential driver of volcanic outgassing due to tidal heating (D. Z. Seligman et al. 2024). An upcoming JWST/MIRI program (GO 6457) will search for the presence of an outgassed atmosphere for LP 791-18 d using secondary eclipse observations, but the predicted tidal heat flux and volcanic outgassing rate depends in part on the orbital eccentricity, and the predicted timing of these eclipses depends sensitively on the assumed orbital eccentricity and longitude of periastron.

The precision of the current mass and eccentricity constraints for LP 791-18 d are limited by the relatively small amplitude of the TTVs (~ 40 s) that it induces on the much more massive planet c. Among the ensemble of transit timing measurements presented in P23, the Spitzer observations were the only ones precise enough to detect these timing variations, and as a result they drive the TTV constraints for both planets. In this study, we utilize diffuser-assisted infrared transit photometry with the Wide-field InfraRed Camera (WIRC; S. Vissapragada et al. 2020) at Palomar Observatory to observe three new transits of LP 791-18 c. With this setup, we achieved a timing precision superior to that of Spitzer.

In Section 2, we describe our transit follow-up observations. In Section 3, we describe our TTV modeling and analysis. In Section 4, we discuss our results, and in Section 5 we summarize our key findings.

2. Transit Follow-up

2.1. Palomar/WIRC Observations

We observed three transits of LP 791-18 c in the *J* band with WIRC on the 200" Hale Telescope at Palomar Observatory, California, USA. The Hale Telescope is a 5.08 m telescope equipped with a 2048 x 2048 Rockwell Hawaii-II NIR detector, providing a field of view of 8.7×8.7 with a plate scale of $0''.25$ per pixel (WIRC; J. C. Wilson et al. 2003). Our data were taken with a beam-shaping diffuser that increased our observing efficiency and improved the photometric precision and guiding stability (G. Stefansson et al. 2017; S. Vissapragada et al. 2020).

We observed transits of LP 791-18 c on UT 2023 December 9, 2024 January 8, and 2024 May 12. We used 10 s exposure times stacked to 4 total coadded exposures per image, and observed full transits plus at least 1 transit duration of baseline (Figure 1). Exposure time is typically varied on the night of observation based on the sky conditions (Moon fraction and proximity, cloud cover, etc.), but we found 40 s total exposure time to be sufficient for all observations. For each night, we obtained calibration images to dark subtract, flat field, remove dead and hot pixels, and remove detector structure with a nine-point dithered sky background frame following the methodology of S. Vissapragada et al. (2020). We extracted photometry for our target star and a set of nearby comparison stars, and we chose up to 10 comparison stars that have minimal variance relative to the time-changing flux of the target star. For the UT 2024 January 8 and 2024 May 12 observations, these were the same eight comparison stars, while for the UT 2023 December 9 observation we used two additional comparison stars for a total of 10. The final number of comparison stars was decided by the significance of their weights in the fitting procedure described in Section 2.2. We cleaned the target and comparison light curves by applying a moving median filter with a width of 31 data points and removing 5σ outliers. We then

Table 1
Summary of Ground-based Palomar/WIRC Observations of LP 791-18 c

| UT Date | Start | Finish | Transit % | Baseline % | z_{st} | z_{min} | z_{end} | Transit Midtime (BJD; Section 2.2) |
|-------------|----------|----------|-----------|------------|----------|-----------|-----------|------------------------------------|
| 2023 Dec 9 | 10:31:42 | 12:44:43 | 100% | 105% | 2.54 | 1.60 | 1.60 | 2460287.987952 ± 0.000070 |
| 2024 Jan 8 | 08:18:33 | 11:06:46 | 100% | 140% | 2.84 | 1.57 | 1.57 | 2460317.927413 ± 0.000050 |
| 2024 May 12 | 03:32:42 | 06:06:23 | 97% | 120% | 1.55 | 1.55 | 2.15 | 2460442.675472 ± 0.000037 |

Note. Start and Finish columns represent the time of first and last science images in UT time, the transit and baseline fractions are relative to the total transit duration for LP 791-18 c, z_{min} is the minimum air mass of the science sequence while z_{st} and z_{end} are the starting and ending air masses.

tested various target aperture sizes from 5 to 25 pixels and selected the optimal aperture by minimizing the root mean square scatter after the light-curve fitting described in Section 2.2. Our optimal apertures were 19, 19, and 12 pixels for UT 2023 December 9, 2024 January 8, and 2024 May 12, respectively. For the UT 2023 December 9 observation we experienced poor seeing approaching the 3'' width of our diffuser and intermittent partial cloud cover, and for the UT 2024 January 8 observation we experienced poor seeing below 3''. This affected our photometric precision and target PSF width, but we do not exclude any data from these observations because the comparison star fluxes still track very closely with the target star flux resulting in strong transit detections (Figure 1). Additional information about our transit observations, including observation times, transit coverage, and air masses, are provided in Table 1.

2.2. Transit Modeling

We fit the WIRC light curves using exoplanet with a combined systematics and transit model as described in M. Greklek-McKeon et al. (2023). Our systematics model for each night included a linear combination of comparison starlight curve weights, an error inflation term added in quadrature to the flux errors, and a linear slope. We also tested systematics models with linear combinations of weights for the target centroid offset, PSF width, air mass, and local sky background as a function of time. We compared the Bayesian Information Criterion (BIC; G. Schwarz 1978) for all possible combinations of these systematic noise parameters using the same framework as in J. Pérez-González et al. (2024). We found that the model that produced the lowest BIC value included weights for the target PSF width on UT 2024 January 8, while our UT 2023 December 9 and 2024 May 12 observations preferred no additional detrending parameters in the systematics model. When optimizing the systematics model for each night, we also fit for the transit shape parameters (impact parameter b , planet-star radius ratio R_p/R_* , and semimajor axis ratio a/R_*), and found that they were all consistent within 1σ across all three nights.

We fit the three WIRC transits jointly (Figure 1). We used the same model framework as in M. Greklek-McKeon et al. (2023), with a wide uniform prior of ± 2 hr on the transit times, transit shape parameters (impact parameter b , planet-star radius ratio R_p/R_* , semimajor axis ratio a/R_*) shared across nights, with different systematics model parameters and comparison star weights for each night. We adopted stellar parameters from P23 and used `ldtk` (H. Parviainen & S. Aigrain 2015) to calculate the J -band quadratic WIRC limb-darkening parameters $u_1 = 0.182$ and $u_2 = 0.151$, and held them fixed in our fits. We explored the parameter space with the NUTS sampler in PyMC3 for 2500 tune and 2000 draw

steps with four chains, and confirmed that the chains have evolved until the Gelman-Rubin statistic values are <1.001 for all parameters. Our measured transit times are listed in Table 1, and the final transit light curves are shown in Figure 1. We achieved transit timing precisions of 6, 4, and 3 s for our Palomar/WIRC transits of LP 791-18 c. This represents an improvement over the 9 s transit timing precision of the two Spitzer transits of planet c presented in P23.

3. TTV Modeling

3.1. Validation of TTV Model and Choice of Eccentricity Parameterization

Before performing an updated TTV model fit using our new transit times, we first fit the original set of transit times listed in Extended Data Tables 1 and 2 of P23, where we independently reproduced their solution. We used the TTVFast package to model the observed transit times. TTVFast (K. M. Deck et al. 2014) is a computationally efficient n -body code that uses a symplectic integrator with a Keplerian interpolator to calculate transit times in multiplanet systems. The modeled transit times are a function of the planetary mass ratios and orbital elements relative to a reference epoch, which we chose to be $T_0 = 8546.0$ (BJD-2450000), the same as P23. In our TTV modeling, we also fixed the planetary orbital inclinations (i) to 90° , since the transit fits indicate that planets d and c have a low mutual inclination and are very close to edge on ($i_d = 89.34 \pm 0.41$, $i_c = 89.78 \pm 0.13$, P23). For a purely edge-on orbital inclination the longitude of the ascending node (Ω) becomes undefined, so we arbitrarily set it to 90° for both planets. The TTV model also includes the planet-to-star mass ratios (M_p/M_*), Keplerian orbital periods (P), mean anomalies reparameterized with the time of first transit (t_0), and the planetary eccentricities (e) and longitudes of periastron (ω). This results in a total of ten free parameters in our two-planet TTV model. Prior distributions used for these model parameters are described in Table 2. Also as in P23, we did not include planet b in the TTV analysis because the predicted amplitude of its TTVs and its predicted impact on the TTVs of planets c and d are less than one second, independent of the planet masses. Following P23, we initially fit the data with e and ω parameterized as $\text{ecos}(\omega)$ and $\text{esin}(\omega)$ (J. Eastman et al. 2013). As originally noted by E. B. Ford (2006), fitting for $\text{esin}(\omega)$ and $\text{esin}(\omega)$ results in an effective linear prior on e , which must be corrected by weighting the stepping probability by e_{i-1}/e_i , where the subscript i denotes the current link in the chain. This approach has been used in previous TTV studies (e.g., E. Agol et al. 2021), and was the approach adopted by P23, so we use it as well.

Table 2
Priors and Posteriors for LP 791-18 Model Parameters

| Parameter | Prior | Posterior |
|---|---------------------------------------|---|
| <i>Measured Planetary Parameters, Palomar/WIRC Transit Fit (Section 2.2)</i> | | |
| a/R_\star | $p(a/R_\star P, M_\star, R_\star)$ | <i>LP 791-18 c</i> $37.05^{+0.05}_{-0.07}$ |
| R_p/R_\star | $\mathcal{U}(0.0, 0.2)$ | $0.12518^{+0.00027}_{-0.00027}$ |
| Impact parameter, b | $\mathcal{U}(0, 1 + R_p/R_\star)$ | $0.0367^{+0.0323}_{-0.0222}$ |
| <i>Measured Planetary Parameters, TTV fit, Nondamped Free Eccentricity Prior (Section 3.3)</i> | | |
| P (days) | $\mathcal{U}(P-1.0, P+1.0)^a$ | <i>LP 791-18 d</i> $2.75519^{+0.00044}_{-0.00046}$ |
| t_0 (BJD–2458540) | $\mathcal{U}(t_0 - 2.5, t_0 + 2.5)^b$ | <i>LP 791-18 c</i> $4.98987^{+0.00006}_{-0.00007}$ |
| $\sqrt{e} \cos \omega$ | $\mathcal{U}(-1, 1)$ | $6.37773^{+0.00068}_{-0.00065}$ |
| $\sqrt{e} \sin \omega$ | $\mathcal{U}(-1, 1)$ | $-0.120^{+0.056}_{-0.048}$ |
| $M_p/M_\star \times 10^{-6}$ | $\mathcal{U}(0, 90)$ | $0.115^{+0.056}_{-0.086}$ |
| <i>Measured Planetary Parameters, TTV fit, Damped-state Free Eccentricity Prior (Section 3.2)</i> | | |
| P (days) | $\mathcal{U}(P-1.0, P+1.0)^a$ | <i>LP 791-18 d</i> $2.75485^{+0.00013}_{-0.00013}$ |
| t_0 (BJD–2458540) | $\mathcal{U}(t_0 - 2.5, t_0 + 2.5)^b$ | <i>LP 791-18 c</i> $4.9899100^{+0.0000012}_{-0.0000014}$ |
| $\sqrt{e} \cos \omega$ | $\mathcal{U}(-1, 1)$ | $6.37888^{+0.00037}_{-0.00038}$ |
| $\sqrt{e} \sin \omega$ | $\mathcal{U}(-1, 1)$ | $-0.0033^{+0.0266}_{-0.0262}$ |
| $M_p/M_\star \times 10^{-6}$ | $\mathcal{U}(0, 90)$ | $0.0034^{+0.0268}_{-0.0274}$ |
| <i>Derived Planetary Parameters</i> | | |
| Inclination, i (deg) | ... | <i>LP 791-18 d</i> 89.34 ± 0.41^c |
| Semimajor axis, a (au) | ... | <i>LP 791-18 c</i> 0.01992 ± 0.00024^c |
| Planet radius, R_p (R_\oplus) | ... | <i>LP 791-18 d</i> $1.032^{+0.044c}_{-0.043}$ |
| Planet mass, M_p (M_\oplus), [nondamped e prior] | ... | <i>LP 791-18 c</i> 0.98 ± 0.30 |
| Planet mass, M_p (M_\oplus), [damped e prior] | ... | <i>LP 791-18 c</i> 0.91 ± 0.19 |
| Bulk density, ρ (g cm^{-3}), [nondamped e prior] | ... | <i>LP 791-18 d</i> 4.92 ± 1.63 |
| Bulk density, ρ (g cm^{-3}), [damped e prior] | ... | <i>LP 791-18 c</i> 4.56 ± 1.12 |
| Eccentricity, e , [undamped e prior] | ... | <i>LP 791-18 d</i> $0.056^{+0.015}_{-0.014}$ |
| Eccentricity, e , [damped e prior] | ... | <i>LP 791-18 c</i> $0.0011^{+0.0010}_{-0.0008}$ |

Notes.^a Centered on the reported period values of P23.^b Centered on the reported t_0 values of P23, adjusted for BJD–2458546.^c Value from M. S. Peterson et al. (2023).

The orbital periods, mean anomalies, eccentricities, and longitudes of periastron are osculating orbital elements defined at the TTV model start time T_0 . Along with this TTV model parameterization, we incorporated the damped-state free eccentricity prior described in P23. This study performed long-term n -body simulations with REBOUND (H. Rein & D. Tamayo 2015), which indicated that the eccentricities of the planets should be damped to values near zero (~ 0.001 for d, and ~ 0.0001 for c) on relatively short timescales (see Section 3.2 for additional analysis of this). These damped-state eccentricities oscillate around stable long-term equilibria, and represent the forced eccentricities that are preserved due to mutual gravitational interactions between the planets after the free eccentricity has been stripped away by tidal damping. P23 implemented this damped-state prior on the eccentricities by computing the free and forced eccentricity components for planets c and d for each proposed step in the Markov chain Monte Carlo (MCMC) using a two year REBOUND simulation, and then imposing Gaussian priors on the values of the free

eccentricities centered at zero and with a standard deviation of 0.001 for planet d and 0.0001 for c. We found that we obtained equivalent results using REBOUND simulations with a duration of 6 months rather than the two years utilized by P23 and adopted this approach in order to decrease the run time of our fits. This had the added advantage of making sure that our estimate of the forced eccentricity was not biased by the long-term osculations of the free eccentricity term, while still accurately separating the free versus forced eccentricity components by simulating many of the 26 day TTV super-periods of LP 791-18 d and c (P23).

We fit our TTV model to the data from P23 using the affine invariant MCMC ensemble sampler emcee (D. Foreman-Mackey et al. 2013), and chose wide uniform priors for all parameters: $\mathcal{U}(-1, 1)$ for $\text{ecos}(\omega)$ and $\text{esin}(\omega)$, $\mathcal{U}(0, 30M_\oplus)$ for the planet-star mass ratios, $\mathcal{U}(P-100\sigma, P+100\sigma)$ for the planetary orbital periods, and $\mathcal{U}(t_0-100\sigma, t_0+100\sigma)$ for the t_0 parameters using the period and $t_0\sigma$ values for each parameter reported in P23, in addition to the damped-state free

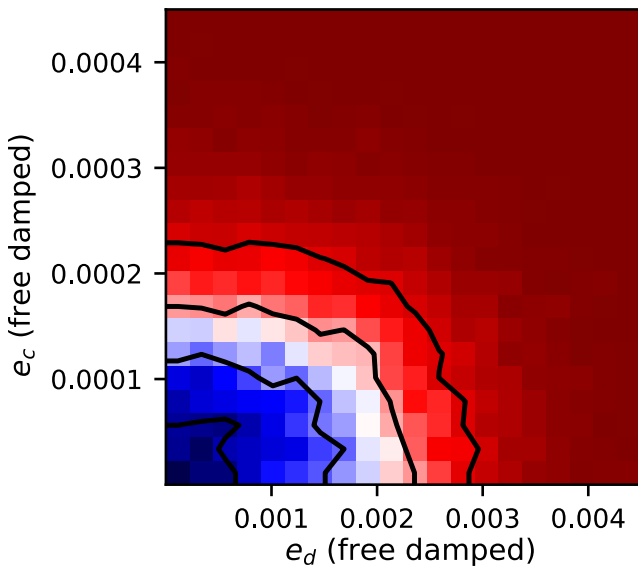


Figure 2. The posterior probability density distribution of planetary eccentricities for LP 791-18 d and c with a fit to the TTV data of P23 using a tidally damped-state eccentricity prior and parameterizing e and ω as $\sqrt{e} \cos(\omega)$ and $\sqrt{e} \sin(\omega)$.

eccentricity prior. We initialized the MCMC fit with 200 walkers (20 per free parameter) randomly distributed across the full prior volume. We ran the sampler for 7000 steps, which is more than 50 autocorrelation lengths for all parameters after discarding the initial 1500 steps as burn in. We obtained results consistent within 1σ to those reported in P23 for all fit parameters with this damped-state eccentricity model framework. When we repeated the TTV analysis without the damped-state eccentricity prior, we also obtained planetary mass values consistent with those reported in P23.

Next, we repeated our fit to the TTV data from P23 with an alternative parameterization for e and ω . The correction method used to eliminate the effective positive linear prior in e for the $e\cos(\omega)$ and $e\sin(\omega)$ parameterization described in E. B. Ford (2006) and utilized by P23 preferentially rejects steps with higher eccentricity and results in an approximately but not perfectly uniform prior in e . Due to the singularity at $e = 0$, there is a very slight overcorrection as e approaches zero, as can be seen in J. Eastman et al. (2013)'s Figure 1. For this reason, J. Eastman et al. (2013) recommend using the $\sqrt{e} \cos(\omega)$ and $\sqrt{e} \sin(\omega)$ parameterization, which naturally recovers a uniform prior in e and ω . When we repeated our fit to the P23 data using this parameterization, we found that the small but nonzero eccentricities reported by P23 ($e_d = 0.0015 \pm 0.00014$ and $e_c = 0.0008 \pm 0.0004$) for planets d and c vanished and we instead retrieved eccentricity posteriors consistent with zero for both planets (Figure 2). When we compared this tidally damped eccentricity fit to one where we forced $e = 0$ for both planets, the difference in best-fit predicted transit times is less than 1 s for both planets, compared to our smallest transit timing precision of 3 s. This confirms that the observational data are not sensitive to eccentricities this small (~ 0.001), and the originally reported values from P23 were an artifact of the chosen e and ω parameterization. In order to avoid this bias, we use the $\sqrt{e} \cos(\omega)$ and $\sqrt{e} \sin(\omega)$ parameterization in all of our TTV model fits going forward.

3.2. The Damped Case

We performed an updated TTV fit using the TTV observations from P23 and our three new transit observations of LP 791-18 c, applying the same free eccentricity tidally damped-state prior described in Section 3.1. We ran the TTV MCMC retrieval with 200 walkers for 25,000 steps, ensuring that all parameters achieved >50 autocorrelation lengths. We show the updated suite of TTV observations in Figure 3, with a representative sample of TTV model fits overplotted and a comparison to the nondamped free eccentricity TTV retrieval shown. We found that the TTV-based eccentricities remain consistent with zero when applying the damped-state eccentricity prior (see Figure 4). This has significant implications for the tidal heat flux of LP 791-18 d, as discussed in Section 4.1. Our updated planet masses are consistent with those reported in P23, but with an improvement in the fractional mass uncertainty for LP 791-18 d from $\sim 45\%$ to $\sim 20\%$. We discuss the corresponding implications for the interpretation of this planet's bulk density in Section 4.3.

3.3. The Nondamped Case

In order for the tidal circularization timescale (A. Puranam & K. Batygin 2018, Equation (1)) to be comparable to or longer than the age of the system (>0.5 Gyr, P23), the reduced tidal quality factor Q' (defined as Q/k_2) must be $\geq 10^4$ for LP 791-18 d. This value would be similar to the super-Earth GJ 876 d, whose nonzero eccentricity is maintained by chaotic excitations from nearby planets (A. Puranam & K. Batygin 2018), but much larger (and less dissipative) than the values commonly assumed for terrestrial planets (10–100, N. Clausen & A. Tilgner 2015). For LP 791-18 c, $Q_c \geq 7 \times 10^3$ would yield a circularization time comparable to the system age. This is consistent with predictions of the range of Q_p values for sub-Neptune exoplanets from interior modeling and population-level analysis (e.g., P. Goldreich & S. Soter 1966; N. Nettelmann et al. 2011; N. Clausen & A. Tilgner 2015; G. Tobie et al. 2019; E. M. Louden et al. 2023) and smaller (more dissipative) than measured values for Neptune-sized exoplanets (e.g., GJ 436 b, $Q_p = 2 \times 10^5$ – 10^6 , C. V. Morley et al. 2017). We caution that if LP 791-18 is considerably older than 1 Gyr, both planets would require higher Q_p values and much less efficient tidal dissipation to retain any free eccentricity. It is therefore likely that LP 791-18 d has a damped free eccentricity based on the predictions of Q_p values for terrestrial planets, but a much larger Q_p also cannot be ruled out.

We explore this possibility by performing an updated TTV fit including our Palomar/WIRC observations for the case with a free eccentricity prior. In this case, we used the same TTV model parameterization as before, with a uniform prior from -1 to 1 on $\sqrt{e} \cos(\omega)$ and $\sqrt{e} \sin(\omega)$, but without the additional damped-state free eccentricity prior. We ran this MCMC retrieval with 200 walkers for 5×10^5 steps, ensuring that our chains extended over more than 50 autocorrelation lengths for each parameter. Without the damped-state prior, which significantly reduces the size of the eccentricity parameter space, this MCMC sampling requires many more steps to fully explore the parameter space as the mass and eccentricity parameters are correlated in the TTV model. The results of this TTV model and the damped-state eccentricity prior TTV retrieval are shown in Figure 4.

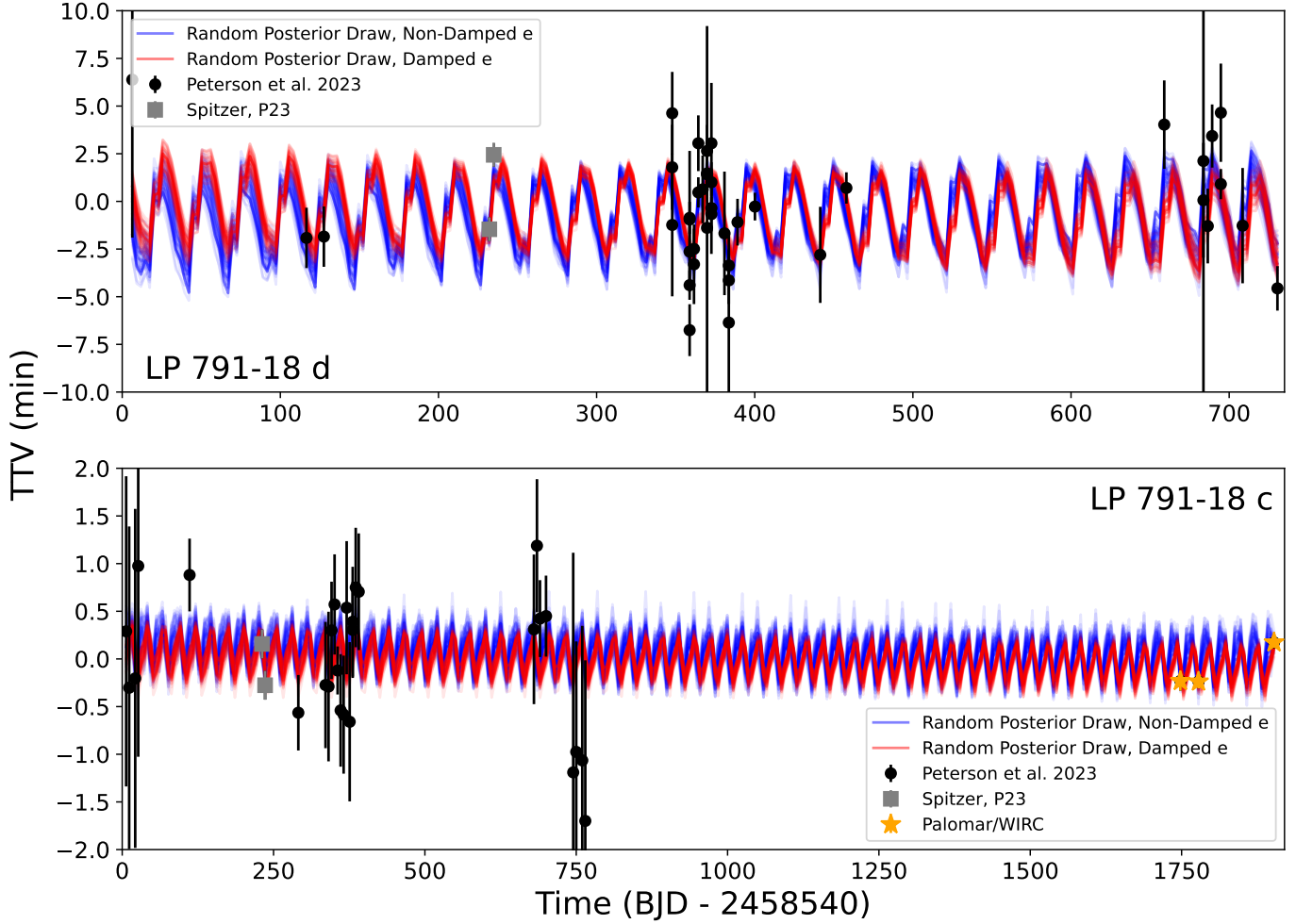


Figure 3. TTVs from the ground-based follow-up campaign of P23 (black circles) including the high-precision Spitzer observations (gray squares), and our new Palomar/WIRC follow-up observations (orange stars), with 100 random posterior draws from our damped eccentricity TTV model (red) and free eccentricity TTV model (blue) for LP 791-18 c (top panel) and d (bottom panel). Our Palomar/WIRC timing measurements for LP 791-18 c are the most precise TTV observations of this system so far, a factor of 1.5–3× more precise than Spitzer, and drive the TTV model constraints for LP 791-18 d.

We find that our undamped fit prefers moderately nonzero eccentricity values for both planets ($e_d = 0.056^{+0.017}_{-0.014}$ and $e_c = 0.062^{+0.017}_{-0.014}$). These higher eccentricities also result in slightly higher masses for both planets, although with larger mass uncertainties and still consistent within 1σ to the fit with a damped eccentricity prior (Figure 4).

The current data cannot differentiate between the damped versus undamped models. We compare the chi-squared values for the maximum likelihood model parameters in the damped versus nondamped eccentricity TTV models, and find that the nondamped χ^2 value is 26% smaller than the damped χ^2 value. This is an insignificant difference in the quality of fit (J. V. Wall & C. R. Jenkins 2012). We discuss the implications of these potentially higher eccentricity and mass values for the tidal heat fluxes and compositions of the planets in Section 4.

4. Discussion

4.1. Tidal Heating Constraints

In the case where LP 791-18 d's free eccentricity is damped and $e_d = 0.0015 \pm 0.00014$ as reported in P23, then the tidal heat flux at the planet's surface is 10^{-3} times the insolation flux. This is still potentially significant for volcanic activity,

however. P23 performs detailed modeling of the planet's internal energy budget in this case, including the effects of silicate melting in the planet's interior, and finds that a tidal heat flux per unit mass similar to Io is probable if LP 791-18 d has an Earth-like mantle composition and rheology. While it is possible that LP 791-18 d maintains this forced eccentricity due to dynamical interactions with LP 791-18 c, we find that the TTV observations are not sensitive to eccentricities this small.

If we instead consider the larger eccentricity value for LP 791-18 d from our nondamped TTV retrieval (Table 2), then the implied tidal heat flux would be much higher than previously reported in P23, with significant implications for the potential outgassing of a secondary atmosphere. In this scenario, the tidal heat flux at the surface of LP 791-18 d increases to a value comparable to the insolation flux, and the tidal heat flux per unit mass jumps by more than 3 orders of magnitude (see Figure 5). Using Equation (1) from S. Millholland et al. (2020), we calculate a corresponding $T_{\text{int}} \approx 145$ K for $Q_d = 10^4$, compared to a planetary T_{eq} of 395 K. In this scenario LP 791-18 d would be comparable to L 98–59 d in terms of tidal heat flux per unit mass (O. D. S. Demangeon et al. 2021; D. Z. Seligman et al. 2024).

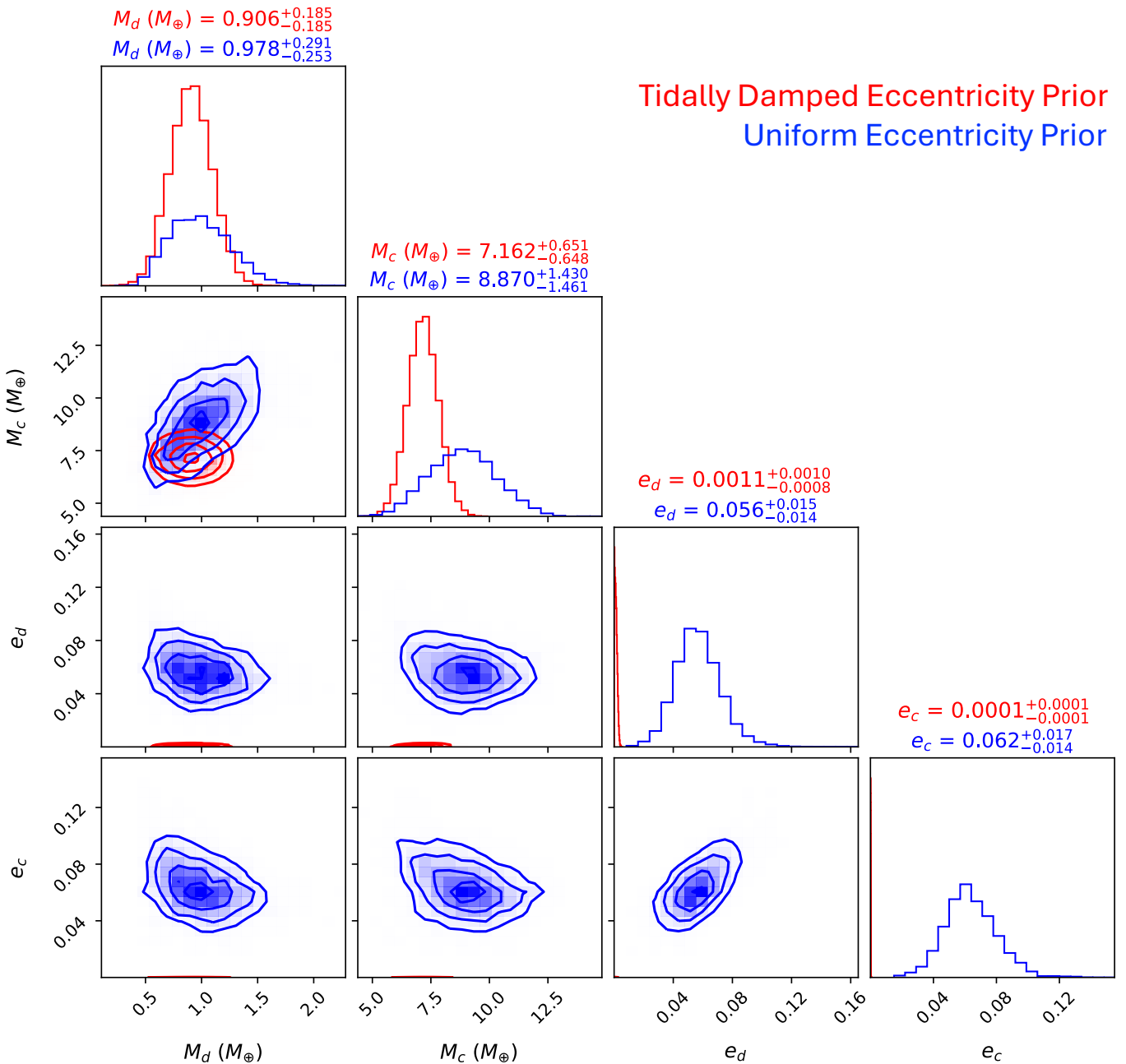


Figure 4. Posterior distributions for the masses and eccentricities of LP 791-18 d and c from a fit to the updated set of TTV observations in the case of a tidally damped free eccentricity prior (red), and a uniform eccentricity prior (blue). If we assume that the eccentricities are damped, then the observations are consistent with $e = 0$ and the planetary masses are slightly lower. If the eccentricities are not damped, the planetary masses are slightly higher.

4.2. Impact on Secondary Eclipse Timing

The predicted timing offset of the secondary eclipse relative to the prediction for a planet on a circular orbit is given by $\Delta t = 2P e \cos \omega / \pi$ (D. Deming et al. 2005). This means that if the higher eccentricity for LP 791-18 d preferred by our free retrieval is correct, it could result in a significantly larger timing offset than the damped-state prediction. This has potentially significant implications for upcoming JWST secondary eclipse observations of this planet in program GO 6457, which have a duration of 4.62 hr per observation, with five total eclipse observations currently scheduled. In Figure 6, we compare the distribution of predicted eclipse timing offsets for LP 791-18 d from the tidally damped and free eccentricity

TTV retrievals. Notably, with $e_d = 0.056 \pm 0.015$, the most probable eclipse timing offset is nearly two hours earlier than the value for the damped fits, with a 1σ uncertainty window of approximately 45 minutes in either direction. This means that it is possible that the secondary eclipse could occur prior to the start of the JWST observing window. In contrast to this prediction, our tidally damped fit predicts an eclipse timing offset of $-0.2^{+2.0}_{-2.7}$ minutes. If this JWST program detects eclipses of planet d with a measured timing offset of more than 10–15 minutes, it would provide direct observational confirmation that this system is not in the tidally damped equilibrium state. There are no currently scheduled eclipse observations of LP 791-18 c, but the equivalent eclipse timing

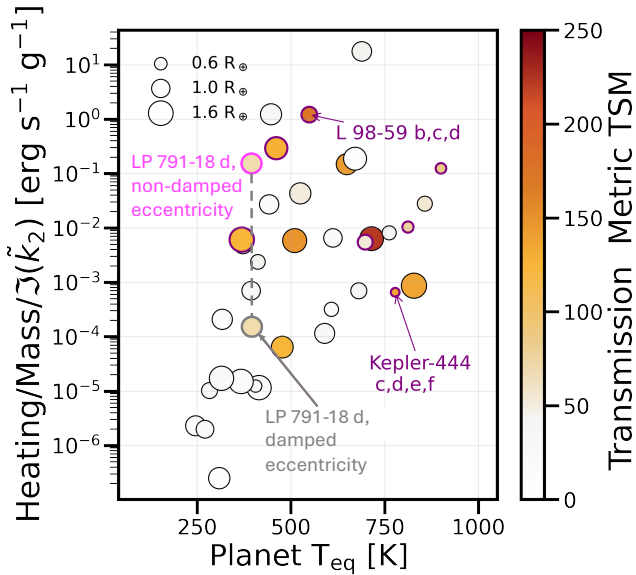


Figure 5. Planetary equilibrium temperature vs. tidal heat flux per unit mass, adapted from Figure 5 of D. Z. Seligman et al. (2024), showing the most promising rocky planets for tidal volcanism. Heat fluxes are normalized by the uncertain tidal quality parameters, point sizes are scaled by planet size, and color indicates the favorability for atmospheric characterization through transmission spectroscopy (E. M. R. Kempton et al. 2018). The difference in tidal heat flux per unit mass for LP 791-18 d spans more than three orders of magnitude for the damped vs. nondamped eccentricity states.

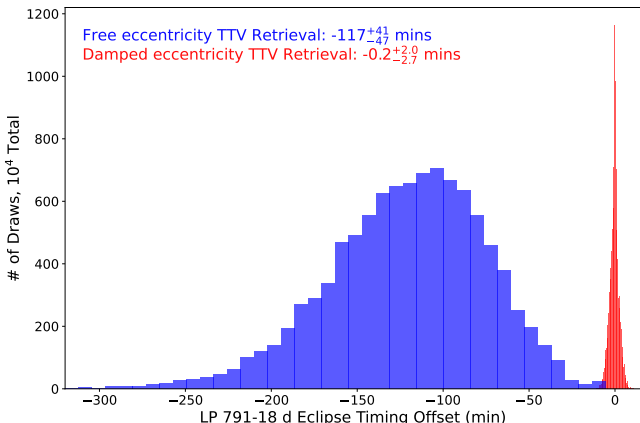


Figure 6. Distributions for the eclipse-timing offsets of LP 791-18 d, using 10^4 draws from the period, e , and ω distributions of the planets in the damped (red) and nondamped (blue) free eccentricity TTV retrievals.

offset distributions for the nondamped and damped-state eccentricities are -273^{+66}_{-81} minutes and $0.0^{+0.3}_{-0.4}$ minutes, respectively.

4.3. Bulk Density Constraints

Our new Palomar transit observations of planet c reduce the uncertainty on the planet-to-star radius ratio (R_p/R_*) by nearly 4× relative to the value reported in P23. Unfortunately, most of the current uncertainty in the planet radius is driven by the stellar radius uncertainty, so our updated planet radius value (shown in Table 2) is only minimally shifted relative to P23. Our mass constraint for the tidally damped case is similar to the value reported by P23, although we prefer a slightly higher mass value for the free eccentricity fit as discussed in Section 3.3. As noted by P23, this planet must have a modest

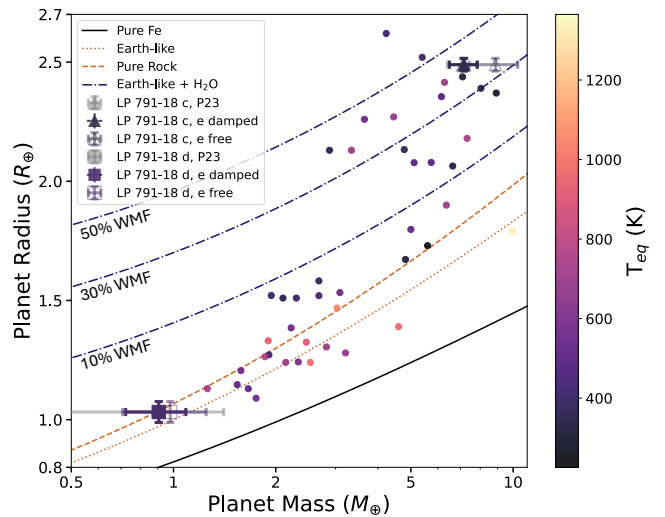


Figure 7. Mass–radius diagram for LP 791-18 d (square) and c (triangle), with updated measurements from this work (filled markers from the damped eccentricity TTV results, open markers for the free eccentricity TTV results) compared to the mass constraints from P23 (gray markers). Filled circles represent all small ($<3 R_⊕$) planets orbiting M dwarfs ($T_* < 3900$ K) with masses and radii measured to better than 3σ , based on the NASA Exoplanet Archive list of confirmed planets as of 2024 November. The predicted equilibrium temperatures of the planets are indicated by the point color. For comparison, we also plot Earth-like water-rich mass–radius curves (for 10, 30, and 50% water mass fractions) from A. Aguirchene et al. (2021) and pure iron, Earth-like, and rocky iso-density curves from L. Zeng et al. (2016).

hydrogen-rich envelope; this remains true for either of our updated mass values, although the mass fraction of the envelope is slightly lower when we use the higher mass value from the free eccentricity fit ($\sim 2\%$, compared to $\sim 2.5\%$ atmospheric mass fraction for the lower mass from the damped eccentricity retrieval; E. D. Lopez & J. J. Fortney 2014’s Table 2).

Our updated fits also result in a significantly improved mass constraint for LP 791-18 d. P23 reported a mass of $0.9^{+0.5}_{-0.4} M_\oplus$, while we find a value of $0.91 \pm 0.19 M_\oplus$ for the damped case and $0.98^{+0.29}_{-0.25} M_\oplus$ for the free eccentricity case. This allows us to better constrain the planetary bulk density (Figure 7), which we find is consistent with an Earth-like rock-iron composition within 1σ for both the damped and nondamped fits. Our best-fit mass for the tidally damped case is slightly lower than the prediction for an Earth-like bulk composition, while the value from our free eccentricity fit is a close match to an Earth-like bulk density.

5. Summary and Conclusions

In this study, we present updated constraints on the properties of the temperate Earth-sized planet LP 791-18 d, and its sub-Neptune-sized neighbor LP 791-18 c. We collected and analyzed three new transit observations of LP 791-18 c from Palomar Observatory, which extends the TTV baseline by ~ 3 yr and yields the most precise TTV observations of this system to date (6, 4, and 3 s timing precisions). We use these observations and an updated TTV modeling framework to obtain new constraints on the masses and eccentricities of LP 791-18 c and d, and an updated R_p/R_* constraint for LP 791-18 c, which is limited in improving the planet radius constraint by our knowledge of the stellar radius. An updated stellar characterization is beyond the scope of this work, but improved knowledge of the stellar radius for LP 791-18

would result in significant improvements to the radius constraint for LP 791-18 c. We summarize our main conclusions below.

We find that the TTV retrievals with a damped-state eccentricity prior are sensitive to the chosen parameterization for e and ω . When we fit for $e\cos(\omega)$ and $e\sin(\omega)$ following P23, it results in a small but nonzero eccentricity for both planets due to the effective eccentricity prior bias near zero as described in J. Eastman et al. (2013) and E. B. Ford (2006). We eliminate this effect by utilizing the $\sqrt{e}\cos(\omega)$ and $\sqrt{e}\sin(\omega)$ parameterization instead, and find that the TTV observations are consistent with zero orbital eccentricity when a damped-state prior is applied. When we repeat our fits without this damped eccentricity prior, the observed TTVs yield moderate nonzero eccentricities for LP 791-18 d and c ($e_d = 0.056^{+0.015}_{-0.014}$ and $e_c = 0.062^{+0.017}_{-0.014}$). For these eccentricities to be maintained on timescales relevant for the age of the system (>1 Gyr), the tidal quality factors must be larger than is typically assumed for Earth-like planets ($Q_d \geq 10^4$) and super-Neptunes ($Q_c \geq 10^3$), though not outside the range of predicted values from modeling (G. Tobie et al. 2019) or constraints from population level analysis (S. Millholland 2019). It is also possible that any nonzero free eccentricity for LP 791-18 c or d might be caused by a more recent dynamical disturbance such as a stellar flyby.

When using the damped eccentricity prior, we find that the masses of LP 791-18 d and c are consistent with previous constraints reported in P23. However, the addition of our new TTV observations reduces the uncertainty in planet mass for LP 791-18 d by more than a factor of 2. Our updated mass constraint for LP 791-18 d from this fit is lower than an Earth-like value, but still consistent within 1σ . Our free eccentricity TTV retrieval prefers slightly larger masses for both LP 791-18 d and c, making LP 791-18 d potentially more consistent with an Earth-like bulk composition but not fundamentally changing the interpretation of the planetary compositions from bulk density.

Our two fits result in significantly different predictions for LP 791-18 d's tidal heat flux. If the planet's eccentricity is close to zero as suggested by the tidally damped fits, this tidal heat flux would be relatively low, though still potentially significant for the planet's composition and evolution as reported in P23. If the higher eccentricity preferred in the nondamped eccentricity prior fit is correct, the implied tidal heat flux could be orders of magnitude larger. We show that upcoming JWST observations of LP 791-18 d's secondary eclipse can easily differentiate between these two scenarios. As long as the eclipse occurs within the JWST observational window, its timing can be used to obtain a significantly tighter constraint on LP 791-18 d's orbital eccentricity, which will in turn result in improved constraints on the masses of both planets in the TTV fit. If the system is in the tidally damped state, JWST observations will be sensitive to much lower (<0.01) eccentricities than are detectable in the current TTV

data. If JWST instead shows that LP 791-18 d has retained some free eccentricity despite ongoing tidal damping, these observations can be used to constrain its tidal quality factor.

Acknowledgments

We thank the Palomar Observatory telescope operators, support astronomers, hospitality, and administrative staff, without whom this research would not have been possible. We are especially grateful to Paul Nied, Carolyn Heffner, Kathleen Koviak, Diana Roderick, and Rigel Rafto who supported our observations of LP 791-18 c, and to Monastery keeper Jeff Paxton. We thank all of the Palomar Monastery chefs who made observing at Palomar a uniquely pleasant experience, and are sorely missed. Part of this program was supported by JPL Hale telescope time allocations. We are thankful to the PARVI team and Palomar Observatory directorate, especially Chas Beichman, Aurora Kesseli, and Andy Boden for their gracious support of the Palomar TTV survey program during periods requiring quick readjustment of the 200-inch observing schedule.

This research was supported from the Wilf Family Discovery Fund in Space and Planetary Science established by the Wilf Family Foundation. This research has made use of the NASA Exoplanet Archive (NASA Exoplanet Archive 2024b) and the Exoplanet Follow-up Observation Program website, which are operated by the California Institute of Technology, under contract with the National Aeronautics and Space Administration under the Exoplanet Exploration Program. The research made use of the Swarthmore transit finder online tool (E. Jensen 2013).

Facilities: ADS, Exoplanet Archive, TESS, Hale (WIRC).

Software: exoplanet (D. Foreman-Mackey et al. 2021a, 2021b) and its dependencies (Astropy Collaboration et al. 2013, 2018; J. Salvatier et al. 2016; Theano Development Team 2016; D. Foreman-Mackey et al. 2017, 2018; R. Kumar et al. 2019; R. Luger et al. 2019; E. Agol et al. 2020) astropy (Astropy Collaboration et al. 2018), scipy (SciPy 2001), numpy (C. R. Harris et al. 2020), matplotlib (J. D. Hunter 2007), rebound (D. Tamayo et al. 2020), reboundx (T. Lu et al. 2023), BATMAN (L. Kreidberg 2015), emcee (D. Foreman-Mackey et al. 2013), corner (D. Foreman-Mackey 2016), TTVFast (K. M. Deck et al. 2014), lightkurve (Lightkurve Collaboration et al. 2018), and Claude 3.5 Sonnet.

Appendix

Transit Times and Posterior Probability Distributions

Figure 8 shows the full corner plot of the posterior distributions for all model parameters from our TTV fits in the damped and non damped eccentricity cases, while Tables 3 and 4 provide the predicted transit times until 2030 January 1 from our damped and non damped TTV models, respectively.

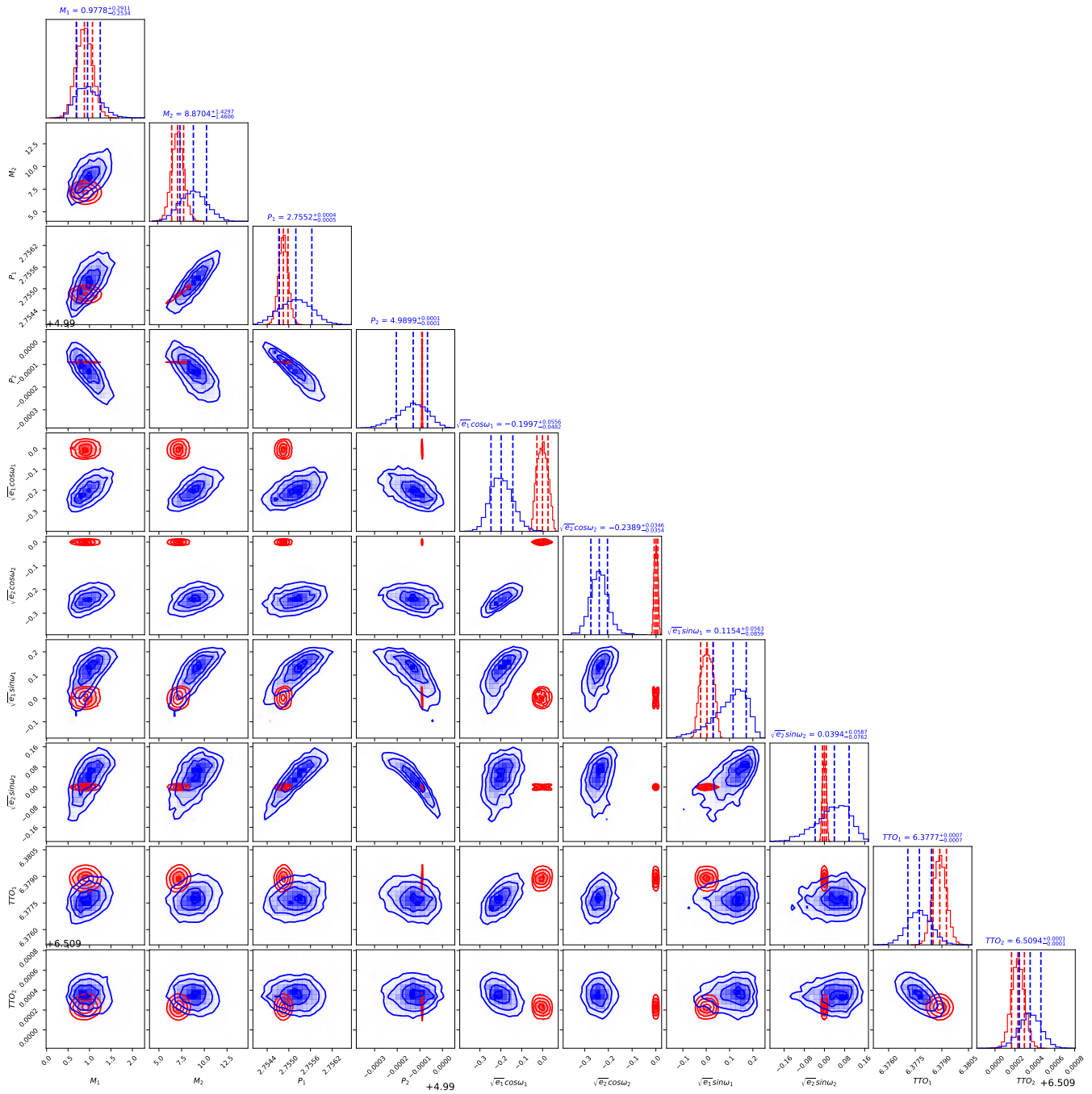


Figure 8. Corner plot of posteriors for TTV model parameters for LP 791-18 d and c from the damped eccentricity (red) and nondamped (blue) versions of the TTV fit, made with the `corner` package (D. Foreman-Mackey 2016). Fit parameters included planet-to-star mass ratios but we have converted these distributions into units of Earth masses for ease of reference. Columns labels are displayed for the undamped fit results.

Table 3

Predicted Transit Times and Uncertainties for LP 791-18 c and d from the TTV Fit with a Tidally Damped Eccentricity Prior, Through 2030 January 1

| Planet | Transit # | Midtime (BJD–2458540) | +1 σ | -1 σ |
|-------------|-----------|-----------------------|-------------|-------------|
| LP 791-18 d | 0 | 6.3789 | 0.0004 | 0.0004 |
| LP 791-18 d | 1 | 9.1314 | 0.0003 | 0.0003 |
| LP 791-18 d | 2 | 11.8842 | 0.0003 | 0.0003 |
| LP 791-18 d | ... | ... | ... | ... |
| LP 791-18 d | 1433 | 3952.0684 | 0.0099 | 0.0117 |
| LP 791-18 d | 1434 | 3954.8219 | 0.0099 | 0.0117 |
| LP 791-18 d | 1435 | 3957.5772 | 0.0101 | 0.0119 |
| LP 791-18 c | 0 | 6.5092 | 0.0001 | 0.0001 |
| LP 791-18 c | 1 | 11.4992 | 0.0001 | 0.0001 |
| LP 791-18 c | 2 | 16.4892 | 0.0001 | 0.0001 |
| LP 791-18 c | ... | ... | ... | ... |
| LP 791-18 c | 789 | 3943.5488 | 0.0020 | 0.0022 |
| LP 791-18 c | 790 | 3948.5389 | 0.0020 | 0.0023 |
| LP 791-18 c | 791 | 3953.5286 | 0.0020 | 0.0022 |

Note. A subset of rows are depicted here for conciseness. The entirety of this table is provided in the arXiv source code.

Table 4

The Same as Table 3, but for the Nontidally Damped Free Eccentricity TTV Fit

| Planet | Transit # | Midtime (BJD–2458540) | +1 σ | -1 σ |
|-------------|-----------|-----------------------|-------------|-------------|
| LP 791-18 d | 0 | 6.3778 | 0.0007 | 0.0007 |
| LP 791-18 d | 1 | 9.1303 | 0.0006 | 0.0006 |
| LP 791-18 d | 2 | 11.8835 | 0.0005 | 0.0004 |
| LP 791-18 d | ... | ... | ... | ... |
| LP 791-18 d | 1433 | 3952.0897 | 0.0678 | 0.0590 |
| LP 791-18 d | 1434 | 3954.8431 | 0.0677 | 0.0589 |
| LP 791-18 d | 1435 | 3957.5981 | 0.0665 | 0.0581 |
| LP 791-18 c | 0 | 6.5093 | 0.0001 | 0.0001 |
| LP 791-18 c | 1 | 11.4992 | 0.0002 | 0.0002 |
| LP 791-18 c | 2 | 16.4892 | 0.0004 | 0.0004 |
| LP 791-18 c | ... | ... | ... | ... |
| LP 791-18 c | 789 | 3943.5464 | 0.1092 | 0.1125 |
| LP 791-18 c | 790 | 3948.5363 | 0.1094 | 0.1126 |
| LP 791-18 c | 791 | 3953.5259 | 0.1095 | 0.1128 |

ORCID iDs

Michael Greklek-McKeon  <https://orcid.org/0000-0002-0371-1647>

Heather A. Knutson  <https://orcid.org/0000-0002-5375-4725>

W. Garrett Levine  <https://orcid.org/0000-0002-1422-4430>

Renyu Hu  <https://orcid.org/0000-0003-2215-8485>

Morgan Saidel  <https://orcid.org/0000-0001-9518-9691>

Jonathan Gomez Barrientos  <https://orcid.org/0000-0002-0672-9658>

Konstantin Batygin  <https://orcid.org/0000-0002-7094-7908>

Björn Benneke  <https://orcid.org/0000-0001-5578-1498>

References

- Agol, E., Dorn, C., Grimm, S. L., et al. 2021, *PSJ*, 2, 1
 Agol, E., Luger, R., & Foreman-Mackey, D. 2020, *AJ*, 159, 123
 Aguchine, A., Mousis, O., Deleuil, M., & Marcq, E. 2021, *ApJ*, 914, 84
 Astropy Collaboration, Price-Whelan, A. M., Sipőcz, B. M., et al. 2018, *AJ*, 156, 123
 Astropy Collaboration, Robitaille, T. P., Tollerud, E. J., et al. 2013, *A&A*, 558, A33
 Banerjee, A., Barstow, J. K., Gressier, A., et al. 2024, *ApJL*, 975, L11

- Clausen, N., & Tilgner, A. 2015, *A&A*, 584, A60
 Crossfield, I. J. M., Waalkes, W., Newton, E. R., et al. 2019, *ApJL*, 883, L16
 Dai, F., Howard, A. W., Halverson, S., et al. 2024, *AJ*, 168, 101
 Deck, K. M., Agol, E., Holman, M. J., & Nesvorný, D. 2014, *ApJ*, 787, 132
 Demangeon, O. D. S., Zapatero Osorio, M. R., Alibert, Y., et al. 2021, *A&A*, 653, A41
 Deming, D., Seager, S., Richardson, L. J., & Harrington, J. 2005, *Natur*, 434, 740
 Eastman, J., Gaudi, B. S., & Agol, E. 2013, *PASP*, 125, 83
 Fischer, D. A., Anglada-Escude, G., Arriagada, P., et al. 2016, *PASP*, 128, 066001
 Ford, E. B. 2006, *ApJ*, 642, 505
 Foreman-Mackey, D. 2016, *JOSS*, 1, 24
 Foreman-Mackey, D. 2018, *RNAAS*, 2, 31
 Foreman-Mackey, D., Agol, E., Ambikasaran, S., & Angus, R. 2017, *AJ*, 154, 220
 Foreman-Mackey, D., Hogg, D. W., Lang, D., & Goodman, J. 2013, *PASP*, 125, 306
 Foreman-Mackey, D., Luger, R., Agol, E., et al. 2021a, *JOSS*, 6, 3285
 Foreman-Mackey, D., Savel, A., Luger, R., et al. 2021b, *exoplanet-dev/* exoplanet, Zenodo, doi:[10.5281/zenodo.1998447](https://doi.org/10.5281/zenodo.1998447)
 Goldreich, P., & Soter, S. 1966, *Icar*, 5, 375
 Greklek-McKeon, M., Knutson, H. A., Vissapragada, S., et al. 2023, *AJ*, 165, 48
 Gressier, A., Espinoza, N., Allen, N. H., et al. 2024, *ApJL*, 975, L10
 Harris, C. R., Millman, K. J., van der Walt, S. J., et al. 2020, *Natur*, 585, 357
 Hunter, J. D. 2007, *CSE*, 9, 90
 Jackson, B., Barnes, R., & Greenberg, R. 2008, *MNRAS*, 391, 237
 Jensen, E. 2013, Tapir: A Web Interface for Transit/eclipse Observability, Astrophysics Source Code Library, ascl:[1306.007](https://ascl.net/1306.007)
 Kempton, E. M. R., Bean, J. L., Louie, D. R., et al. 2018, *PASP*, 130, 114401
 Kreidberg, L. 2015, *PASP*, 127, 1161
 Kumar, R., Carroll, C., Hartikainen, A., & Martin, O. A. 2019, *JOSS*, Lightkurve Collaboration, Cardoso, J. V. d. M., Hedges, C., et al. 2018, Lightkurve: Kepler and TESS Time Series Analysis in Python, Astrophysics Source Code Library, ascl:[1812.013](https://ascl.net/1812.013)
 Lithwick, Y., Xie, J., & Wu, Y. 2012, *ApJ*, 761, 122
 Lopez, E. D., & Fortney, J. J. 2014, *ApJ*, 792, 1
 Loudon, E. M., Laughlin, G. P., & Millholland, S. C. 2023, *ApJL*, 958, L21
 Lu, T., Rein, H., Tamayo, D., et al. 2023, *ApJ*, 948, 41
 Luger, R., Agol, E., Foreman-Mackey, D., et al. 2019, *AJ*, 157, 64
 Millholland, S. 2019, *ApJ*, 886, 72
 Millholland, S., Petigura, E., & Batygin, K. 2020, *ApJ*, 897, 7
 Morley, C. V., Knutson, H., Line, M., et al. 2017, *AJ*, 153, 86
 NASA Exoplanet Archive 2024a, Planetary Systems Composite Parameters, v2024-11-26, NExSci-Caltech/IPAC, doi:[10.26133/NEA13](https://doi.org/10.26133/NEA13)
 NASA Exoplanet Archive 2024b, Planetary Systems, v2024-11-01 12:00, NExSci-Caltech/IPAC, doi:[10.26133/NEA12](https://doi.org/10.26133/NEA12)
 Nettelmann, N., Fortney, J. J., Kramm, U., & Redmer, R. 2011, *ApJ*, 733, 2
 Parviainen, H., & Aigrain, S. 2015, *MNRAS*, 453, 3822
 Pérez-González, J., Greklek-McKeon, M., Vissapragada, S., et al. 2024, *AJ*, 167, 214
 Peterson, M. S., Benneke, B., Collins, K., et al. 2023, *Natur*, 617, 701
 Piaulet-Ghorayeb, C., Benneke, B., Radica, M., et al. 2024, *ApJL*, 974, L10
 Puranam, A., & Batygin, K. 2018, *AJ*, 155, 157
 Quick, L. C., Roberge, A., Mlinar, A. B., & Hedman, M. M. 2020, *PASP*, 132, 084402
 Rein, H., & Tamayo, D. 2015, *MNRAS*, 452, 376
 Salvatiér, J., Wiecki, T. V., & Fonnesbeck, C. 2016, *PeerJ Comput. Sci.*, 2, e55
 Schwarz, G. 1978, *AnSta*, 6, 461
 SciPy 2001, SciPy: Open Source Scientific Tools for Python, <http://www.Scipy.org/>
 Seligman, D. Z., Feinstein, A. D., Lai, D., et al. 2024, *ApJ*, 961, 225
 Stefansson, G., Mahadevan, S., Hebb, L., et al. 2017, *ApJ*, 848, 9
 Tamayo, D., Rein, H., Shi, P., & Hernandez, D. M. 2020, *MNRAS*, 491, 2885
 Theano Development Team 2016, arXiv:[1605.02688](https://arxiv.org/abs/1605.02688)
 Tobie, G., Grasset, O., Dumoulin, C., & Mocquet, A. 2019, *A&A*, 630, A70
 Vissapragada, S., Jontof-Hutter, D., Shporer, A., et al. 2020, *AJ*, 159, 108
 Wall, J. V., & Jenkins, C. R. 2012, Practical Statistics for Astronomers (Cambridge: Cambridge Univ. Press)
 Wilson, J. C., Eikenberry, S. S., Henderson, C. P., et al. 2003, *Proc. SPIE*, 4841, 451
 Wright, J. T. 2018, in Handbook of Exoplanets, ed. H. J. Deeg & J. A. Belmonte (Berlin: Springer), 4
 Zeng, L., Sasselov, D. D., & Jacobsen, S. B. 2016, *ApJ*, 819, 127